Available online at www.sciencedirect.com
SCIENCE DIRECT®
ELSEVIER
Coastal Engineering 50 (2004) 117–138
Coastal Engineering
An International Journal for Coastal, Harbour and Offshore Engineers
www.elsevier.com/locate/coastaleng

Concentrations in oscillatory sheet flow for well sorted and graded sands

Tom O'Donoghue*, Scott Wright

Department of Engineering, King's College, University of Aberdeen, Fraser Noble Building, Aberdeen, AB24 3UE, Scotland, UK

Received 3 December 2002; received in revised form 11 July 2003; accepted 15 September 2003

Abstract

In wave-generated sheet flow conditions, oscillatory near-bed flow is large, ripples are washed out and sand is mainly transported in a thin layer, a few centimetres thick, close to and below the no-flow bed level. New experiments in the Aberdeen Oscillatory Flow Tunnel have produced a comprehensive dataset of transport processes for well-sorted and graded sands in large-scale sinusoidal and asymmetric oscillatory sheet flow conditions. In this paper, detailed time- and height-varying concentration measurements are analysed. The range and level of detail in the measurements make it possible to quantitatively analyse concentration behaviour more rigorously than before. A new empirical equation is presented which characterises the time-dependent concentration profile in the sheet flow layer. The equation involves two time-dependent parameters: erosion depth and reference concentration. The dependence of both parameters on flow and bed conditions is analysed. New results are presented which make it possible to estimate time-dependent erosion depth, reference concentration and, therefore, concentration profile. The effects of grading on sheet flow concentrations are analysed by comparing results from the large range of sand beds tested.

Keywords: Sediment transport; Sheet flow; Waves; Graded sediments; Erosion depth; Reference concentration

1. Introduction

Oscillatory sheet flow occurs when wave-generated near-bed flow velocities are high and sand is transported within a water-sediment mix, a few centimetres deep, moving over a flat ripple-free bed. Sheet flow is important because high sand concentrations are present in the sheet flow layer and very large volumes of sand are transported, so the impact of sheet flow on the overall sediment budget for a coastal area is potentially very large. For this reason a lot of research effort in recent years has been concerned with developing empirical and numerical models of sheet flow processes and transport (Davies et al., 2002). However, the complexity of the underlying mechanics has meant that reliable transport models are not yet available. Confidence in predictive models depends on good agreement between predicted and measured transport rates for controlled conditions, free from scale effects, and, in the case

* Corresponding author. Tel.: +44-1224-272508; fax: +44-1224-272497.
E-mail address: t.o'donoghue@eng.abdn.ac.uk (T. O'Donoghue).

0378-3839/$ - see front matter
doi:10.1016/j.coastaleng.2003.09.004

of process-driven numerical models, good agreement between measured and predicted processes such as time-dependent erosion depths, concentrations, velocities and sediment fluxes.

The present paper focuses on time-dependent sand concentrations in oscillatory sheet flow conditions. Detailed measurements of sheet flow concentrations from large-scale experiments are rare and virtually non-existent for graded sands. Horikawa et al. (1982) were one of the first to measure time-dependent sand concentrations in oscillatory sheet flow. More recently, concentration measurements have come from experiments carried out in the Large Oscillating Water Tunnel (LOWT) at Delft Hydraulics (e.g. Ribberink and Al-Salem, 1995; Katopodi et al., 1994; Chatelus et al., 1998; Dohmen-Janssen, 1999; McLean et al., 2001). These studies have produced very useful data but the resulting descriptions of concentrations in the sheet flow layer have been largely qualitative rather than quantitative. Other previous research includes studies of artificial sediments in oscillatory sheet flow (e.g. Zala-Flores and Sleath, 1998; Sleath, 1999). While these have contributed significantly towards increased understanding of sheet flow processes, direct application of the results to sand in sheet flow conditions is problematic because of differences in fundamental behaviour between sand and the artificial sediments used.

This paper presents detailed oscillatory sheet flow concentration measurements from an experimental programme conducted in the Aberdeen Oscillatory Flow Tunnel (AOFT). The level of detail in the Aberdeen measurements surpasses that of previous research and has led to new insight and quantitative understanding of sheet flow concentration. The experiments cover a wide range of sand beds and include study of graded sands systematically linked to the study of well-sorted sands. The range and level of detail in the new concentration measurements make it possible to analyse concentration behaviour much more rigorously than before. A new equation is presented which characterises the time-dependent sheet flow concentration profile. The equation is based on time-dependent erosion depth and reference concentration and the paper includes analysis of the dependence of these parameters on flow and bed conditions.

2. Experimental set-up

2.1. Facility

The experiments were conducted in the Aberdeen Oscillatory Flow Tunnel (AOFT). The tunnel is fully described in Clubb (2001). It has an overall length of 16 m with a 10-m long glass-sided rectangular test section, 0.75 m high and 0.3 m wide. When a 250-mm deep sand bed is present, test section flow amplitudes of 1.5 m can be produced for periods of 5 s and greater. Sheet flow conditions can, therefore, be generated for a wide range of flows and typical sand sizes. For the present study, a 250-mm deep sand bed occupied the central 6 m of the test section and was bound at either end by marine plywood ramps, fixed to the tunnel floor and sealed to the tunnel sides (Fig. 1). A detailed description of the test set-up is contained in Wright (2002).

2.2. Range of experiments

The experiments involved 7 sands and 4 flows. The sands comprised three well-sorted sands with d_{50} values of 0.15 mm ("fine"), 0.28 mm ("medium") and 0.51 mm ("coarse") and four mixes consisting of different proportions of the well-sorted sands. Table 1 summarises the size characteristics of the different sands. Note that Table 1 contains two values for each size: one is the size obtained using a (Malvern) laser diffraction particle size analyser and the bracketed value is the size obtained using sieve analysis. The sizes differ slightly because the particle size analyser measures a "diameter" which corresponds to the diameter of a sphere of equivalent volume as the particle being measured, while the sieve measures the smaller "diameter" of the particle. The four flows comprised two sinusoidal and two asymmetric flows with periods of 5 and 7.5 s. The properties of the flows are contained in Table 2, as are the codes used to identify each flow condition. The asymmetric flows were based on Stokes 2nd order waves so that $u(t)=u_1 \sin \omega t - u_2 \cos 2\omega t$, with u_1 and u_2 chosen to give flow asymmetry $a=u_{max}/(u_{max}-u_{min})=0.63$ (sinusoidal flows have asymmetry $a=0.5$).

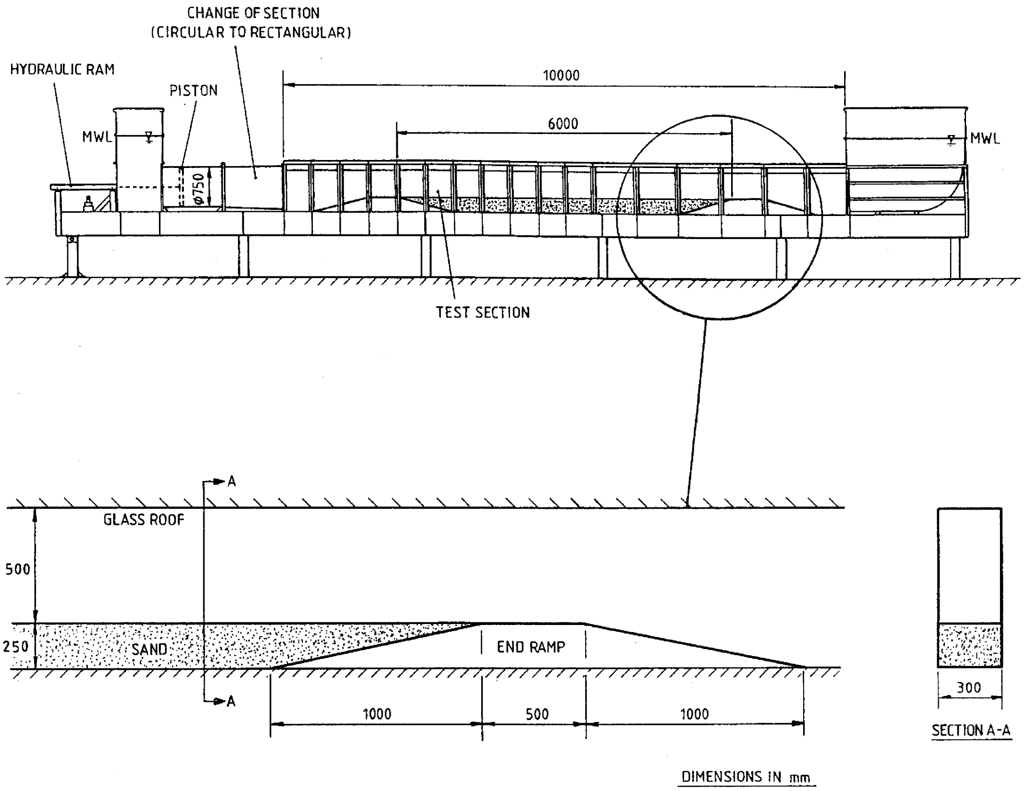

Fig. 1. Aberdeen Oscillatory Flow Tunnel.

2.3. Measurements

The complete experimental programme involved measurement of (i) time-varying concentrations, (ii) time-varying velocities, (iii) net sand transport, (iv) suspended and transported particle size and (v) bed composition. In this paper, we focus on the concentration measurements and specifically on the detailed time-varying concentration measurements in the sheet flow layer. Some of the other aspects of the research are presented in Wright and O'Donoghue (2002).

Two methods were used to measure concentrations. Above the sheet flow layer concentrations were measured using eight transverse suction samplers supplying sediment-laden flow to eight carousels, which rotate with the same period as the oscillatory flow in the tunnel. Each carousel holds a set of 20 bottles so that each bottle collects suspended sediment

Table 1
Size characteristics of the sands used for the experiments (sieve values in brackets)

Name	Mix %F-%M-%C	d_{10} (mm)	d_{50} (mm)	d_{90} (mm)
Fine (F)	100-0-0	0.10 (0.10)	0.15 (0.13)	0.23 (0.17)
Medium (M)	0-100-0	0.17 (0.17)	0.28 (0.27)	0.45 (0.39)
Coarse (C)	0-0-100	0.36 (0.35)	0.51 (0.46)	0.67 (0.58)
Mix1 (X1)	60-30-10	0.11 (0.10)	0.19 (0.15)	0.45 (0.40)
Mix2 (X2)	20-60-20	0.14 (0.12)	0.28 (0.27)	0.53 (0.47)
Mix3 (X3)	35-60-5	0.12 (0.11)	0.24 (0.22)	0.44 (0.39)
Mix4 (X4)	50-0-50	0.11 (0.10)	0.28 (0.26)	0.61 (0.53)

Table 2
Flow conditions

Flow ID	T (s)	A (m)	a	u_{max} (m/s)	u_{rms} (m/s)
Sinusoidal					
512	5	1.2	0.5	1.5	1.1
7515	7.5	1.5	0.5	1.26	0.9
Asymmetric					
A5010	5	1.0	0.63	1.5	0.9
A7515	7.5	1.5	0.63	1.5	0.9

corresponding to a particular 1/20th of the flow period, thereby enabling the time-dependent concentration to be measured. Peristaltic pumps were used to control the flow from each sampler in the tunnel.

Concentrations in the sheet flow layer were measured using conductivity concentration meters (CCMs), similar to those described by Ribberink and Al-Salem (1995). High concentration gradients in the sheet flow layer meant that accurate positioning of the CCM probes was crucial to proper measurement. The exact elevation of the CCM relative to the no-flow bed level ($z=0$) at the start and end of the measurement period was established using the combination of a positioning frame fixed to the underside of the tunnel and a depth gauge deployed through the tunnel roof, as described in Wright (2002). With this set-up, the CCMs could be positioned accurate to the largest grain size on the bed surface. Time-dependent concentration measurement in the sheet flow layer is complicated by the fact that the no-flow bed level can gradually change during the measurement period. An example where the bed change was very large (accreting) is presented in Fig. 2. This shows the generated main flow velocity time-series (Fig. 2a) and the corresponding measured concentration time-series (Fig. 2b) for a CCM that was set at $z=-1$ mm at the beginning of the 12-cycle measurement period but finds itself at $z=-4.8$ mm at the end of the measurement period. The concentration fluctuates strongly at the beginning and is virtually steady by the end of the measurement period. It is important to account for this bed level change in the measurement. To establish the elevation associated with each instantaneous CCM-measured concentration, it was assumed that the bed level varied linearly with time during the course of the measurement period, as illustrated in Fig. 2c. In this way, every concentration measurement was associated with a particular elevation relative to the instantaneous no-flow bed level (i.e. with a particular z) and with a particular phase of the flow cycle (ωt). Combining CCM measurements from all runs involving the same flow and sediment conditions has produced a very large dataset for each flow-sediment combination. The concentration time-series at selected z or the concentration profile at selected phase of the flow cycle can be extracted from each dataset.

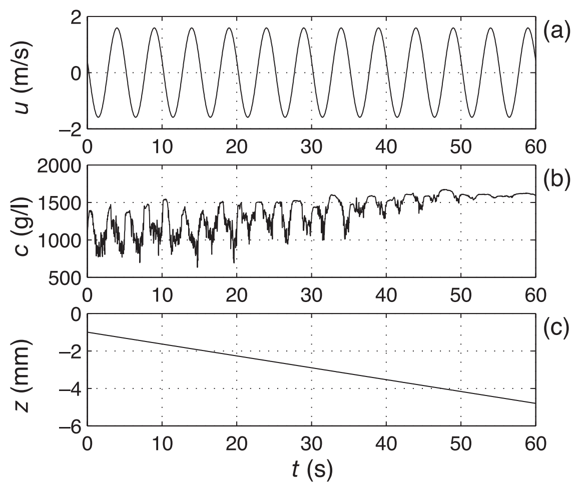

Fig. 2. Example CCM measurement.

3. Sample concentration time-series

Some general features of the measured concentrations are presented here, before the detailed analysis, which follows in later sections of the paper. Fig. 3 presents example measured concentration time-series for the Fine sand in flow 7515, the Mix2 sand in flow A5010, the Medium sand in flow A7515 and the Mix4 sand in flow A5010. The top panel in each case shows the velocity time-history, the bottom panel contains the concentrations measured using the carousel suction sampler system and the 5 panels in between contain the CCM measurements. Each panel contains concentrations corresponding to between 5 and 10 elevations relative to the no-flow bed level ($z=0$) and the range of elevations is indicated in the top left hand corner. The data show the expected decrease in average concentration with increasing elevation above the bed. Also, as expected, in the case of sinusoidal flow, the concentration time-series are more or less symmetric over the onshore (positive) and offshore (negative) flow half-cycles, while concentration time-series are asymmetric in the asymmetric flows.

Within the lower part of the sheet flow layer, concentration decreases as flow velocity increases and sand is picked up by the higher velocity flow; concentration increases again as flow velocity decreases and sand settles back to the bed. This region

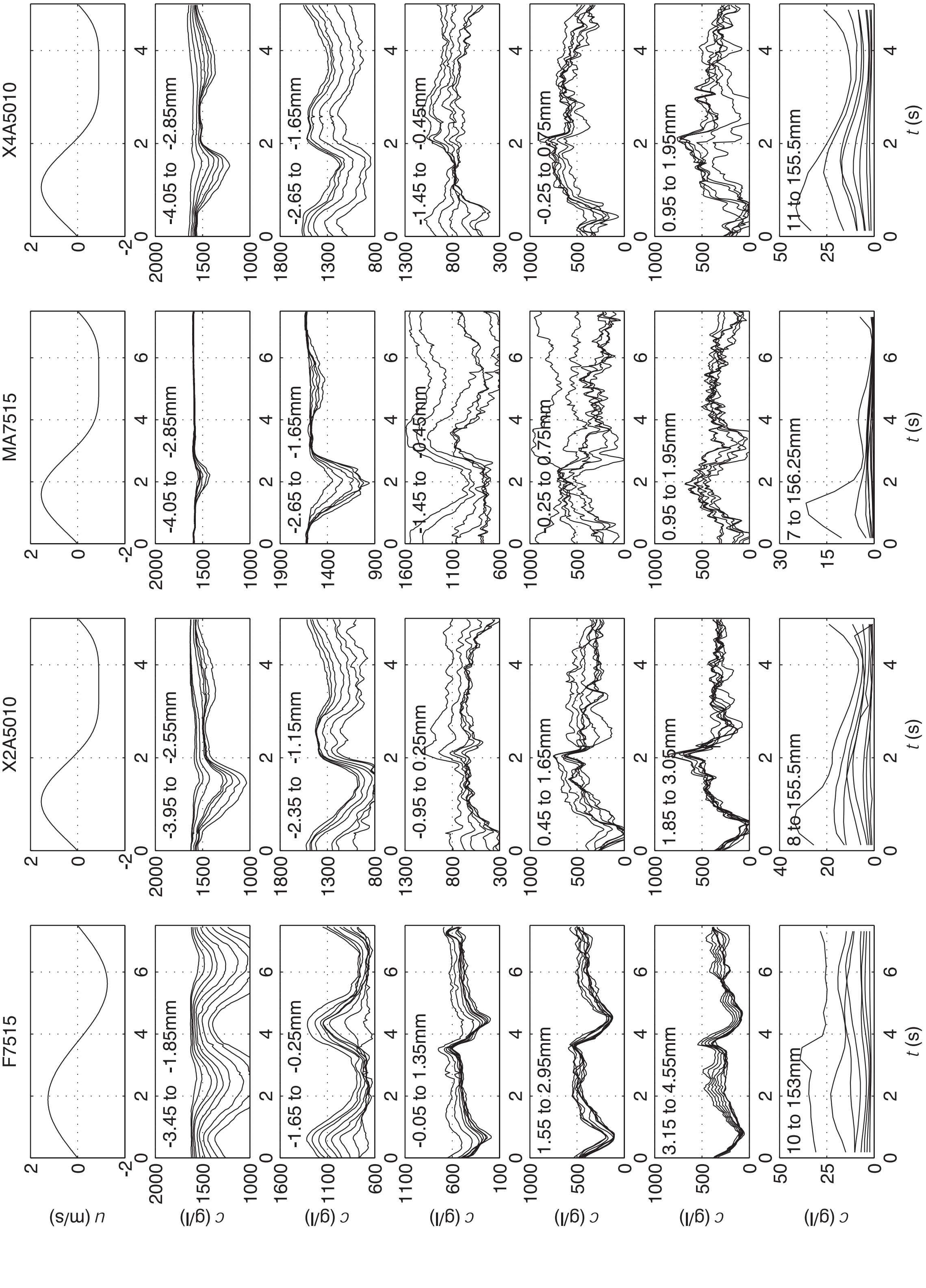

Fig. 3. Example concentration time-series.

of the sheet flow layer, in which time-dependent concentration is approximately in anti-phase with the main flow velocity, is the pick-up layer. A little higher in the flow the dynamic range of concentration is small. This corresponds to the top of the pick up layer and generally occurs at a height where the time-averaged concentration is of the order of 700 g/l. Here, concentrations are maintained by sand rising from below at times of high-flow velocity and sand settling from above at times of low-flow velocity, so that concentration at this level is relatively constant through time. At higher levels in the flow, above the pick-up layer, the concentration time-series tend towards being in phase with the flow velocity, with high concentrations occurring at times of maximum velocity.

Short duration concentration peaks occur at times of flow reversal. The peaks are generally strongest in cases of fine sand and at times of on-offshore flow reversal in asymmetric flows. Similar peaks have been observed in previous studies by, for example, Dohmen-Janssen (1999) where they appear as sharp concentration peaks of short duration at heights above the pick-up layer. The high level of detail in the new concentration measurements shows that the flow reversal concentration peak exists at all levels in the sheet flow layer. Take, for example, the case of the Mix2 sand in flow A5010 (experiment X2A5010): in the upper sheet flow layer (0–3 mm) a well-developed concentration peak occurs near flow reversal at $t \approx 2$ s; the peak decays in magnitude with depth into the sheet flow layer but is still clearly visible in the -2.35 to -1.15 mm panel, well within the pick-up layer.

4. Characterisation of sheet flow concentration profile

Fig. 4 shows CCM-measured concentration profiles for well sorted and three mixed sands at the same instant (maximum onshore velocity) in flow A5010. The concentration has been normalised with respect to the undisturbed bed concentration ($c_0 \approx 1600$ g/l). The results indicate how differently the beds respond to the same flow: note the differences in erosion depth and in profile steepness. Analysis of the entire set of measured instantaneous concentration profiles shows that the profiles are well characterised by an equation of the form:

$$\bar{c}(z,t) = \frac{\beta(t)^{\alpha}}{\beta(t)^{\alpha} + [z + \delta_e(t)]^{\alpha}} \tag{1}$$

where $\bar{c}$ is concentration normalised by sand concentration in the bed, z is elevation above the no-flow bed level and t is time. δ_e is the instantaneous erosion depth and $\bar{c} = 1.0$ at $z = -\delta_e$. For a given α, β describes the instantaneous shape of the concentration profile above the erosion depth: the smaller the value of β, the more rapid the fall-off in concentration with height above the erosion depth. β therefore describes the vertical distribution of entrained sediment; it has dimensions of length and is referred to here as "distribution length". For large z, Eq. (1) tends to the well-known "power law" equation for suspended sediments.

The distribution length β relates directly to reference concentration. From Eq. (1) we can write:

$$\bar{c}(z = z_a, t) = \bar{c}_a = \frac{\beta^{\alpha}}{\beta^{\alpha} + (z_a + \delta_e)^{\alpha}} \tag{2}$$

where $\bar{c}_a$ is normalised reference concentration at reference height $z = z_a$ above the no-flow bed level. (The t has been dropped for ease of presentation in Eq. (2) but it is understood that $\bar{c}_a$, β, α and δ_e are all time-dependent.) Rearranging Eq. (2) gives:

$$\beta = \left\{\frac{\bar{c}_a}{1 - \bar{c}_a}\right\}^{\frac{1}{\alpha}} (z_a + \delta_e) \tag{3}$$

and Eq. (1) for concentration profile can therefore be written

$$\bar{c} = \frac{(z_a')^{\alpha}}{(z_a')^{\alpha} + \left\{\frac{1}{\bar{c}_a} - 1\right\}(z')^{\alpha}} \tag{4}$$

where $z_a' = z_a + \delta_e$ and $z' = z + \delta_e$.

The advantage of Eq. (4) expressed in terms of $\bar{c}_a$ over Eq. (1) expressed in terms of β is that reference concentration, unlike distribution length, is a well-established concept and methods exist for estimating reference concentration for given flow and bed conditions.

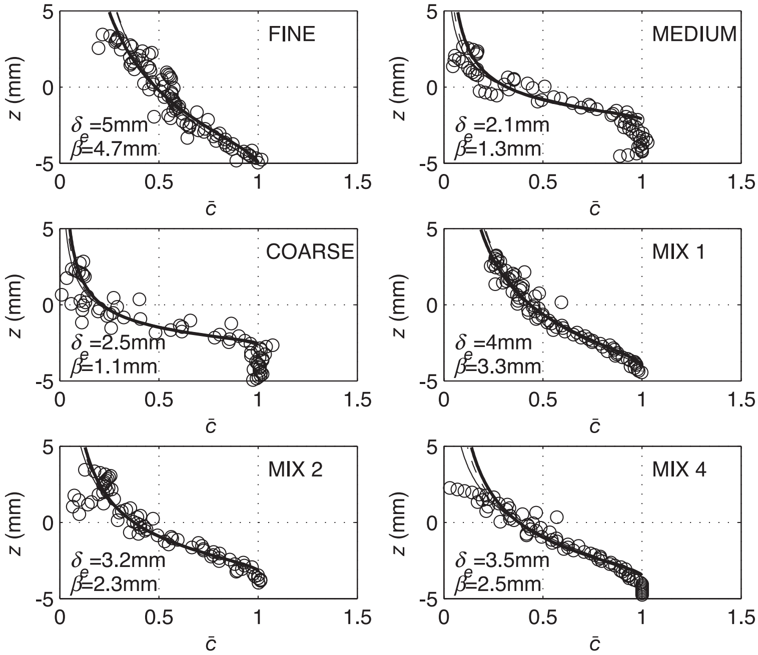

Fig. 4. CCM-measured concentrations (○) and three fits to the measured data (— Fit1; – – Fit2; **—** Fit3) at maximum onshore velocity, experiment A5010.

Fig. 4 includes three fits to the measured concentration profiles. Fit1 is based on Eq. (1) with α, β and δ_e varying in the search for the best fit. Excellent fits to the data are produced but, for some cases, a problem can arise with the value of erosion depth obtained in this way. The problem is illustrated in Fig. 5, which shows the concentration profile at a particular phase of flow A5010 for the coarse sand. The thick black line in Fig. 5 is the result of Fit1 and the corresponding δ_e value is 5.5 mm. However, the actual erosion depth in this case looks to be approximately 3.5 mm. A better estimate of the erosion depth is obtained using the following 2-step procedure: (i) Eq. (1) is fitted to the data with α, β and δ_e varying in the search for the best fit (Fit1); (ii) the point of inflection on the fitted profile is located (see Fig. 5); the straight line through the inflection point, and with slope equal to the slope of the profile at the inflection point, is projected to $\bar{c}=1.0$ to obtain the erosion depth. For the example shown in Fig. 5, this method yields an erosion depth of 3.2 mm. For most cases, the difference between δ_e obtained using Fit1 and δ_e obtained using the 2-step procedure is very small. In some cases, however, particularly cases involving coarse sand (as for the case in Fig. 5), the difference can be substantial.

Fit2 in Fig. 4 is a fit of Eq. (1) to the data but with δ_e values pre-determined using the 2-step procedure described above and with α and β allowed to vary in the search for the best fit. It is seen that the quality of fit to the measured data remains very good. Analysis of α values obtained from Fit2 applied to all of the data showed (i) that α varies little with time for each experiment and (ii) that time-averaged α values from across all experiments lie in the range 1.1–1.9 with a mean value of 1.5. Fit3 in Fig. 4, like Fit2, is a fit of Eq. (1) to the data with δ_e values pre-determined using the 2-step procedure, but in this case α is set constant at a value of 1.5 and only β is varied in the search for the best fit. The results show that setting the constraint $\alpha=1.5$ does not significantly diminish the quality of fit of Eq. (1) to the measured data, particularly in the lower sheet flow layer.

The profile characterisation given by Eq. (4) (or Eq. (1)), with $\alpha=1.5$, provides a very useful vehicle for presenting and analysing the measured concentra-

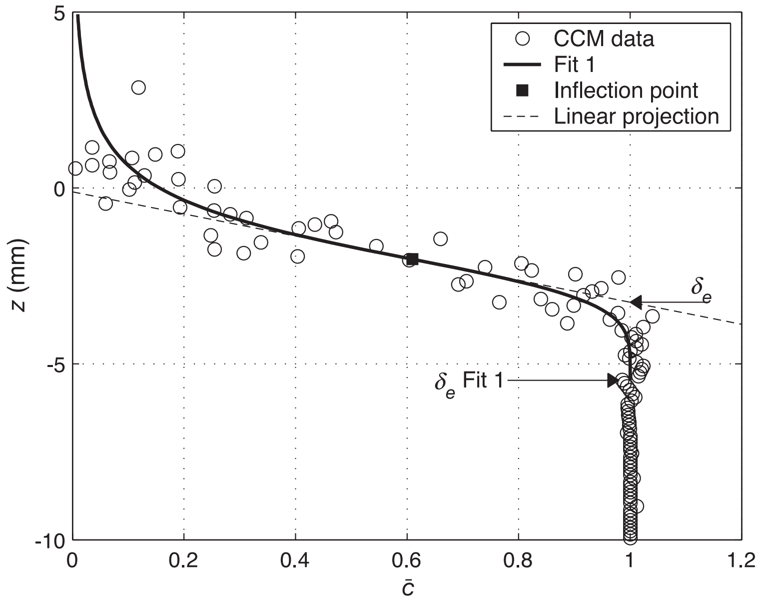

Fig. 5. 2-step method for establishing δ_e.

tion profiles. The instantaneous concentration profile is defined by values of instantaneous erosion depth, δ_e, and instantaneous reference concentration, $\bar{c}_a$ (or distribution length, β). In the following, we examine the measured dependence of these parameters on flow and sand bed conditions.

5. Erosion depth

Measured time-varying δ_e for the sinusoidal and asymmetric flows are presented in Figs. 6 and 7, respectively. Results for the 5 s flows are contained in the left hand column of each figure; the 7.5 s results are contained in the right hand column. Note that maximum flow velocity is lower in the case of the sinusoidal 7.5 s flow than in the case of sinusoidal 5 s flow; maximum velocities are the same in the 7.5 and 5 s asymmetric flows. As might be expected, the δ_e time-histories show two peaks corresponding to the two velocity peaks and the second peak in the case of the asymmetric flows is smaller than the first peak. We observe also that (i) there is a phase difference between the flow and the resulting erosion depth and (ii) δ_e is never zero, even at times of flow reversal when the flow velocity is zero.

The phase lag, ϕ, between the main flow velocity, $u(t)$, and the erosion depth has been calculated for each experiment by cross-correlating $\delta_e(t)$ with $u(t)$. Results for ϕ are presented in Fig. 8, plotted against maximum Shields number, θ_{max} where Shields number is

$$\theta(t) = \frac{\frac{1}{2} f_w u(t)^2}{(s-1) g d_{50}} \text{ and } \theta_{max} = \frac{\frac{1}{2} f_w u_{max}^2}{(s-1) g d_{50}} \tag{5}$$

s is sediment specific gravity (= 2.65 for the sands used), g is acceleration due to gravity and f_w is friction factor. Here we use Wilson et al.'s (1995) method for determining f_w in oscillatory sheet flow conditions. ϕ is seen to increase with increasing θ_{max} in Fig. 8. Note that because of boundary layer effects, it is estimated that the near-bed flow velocity leads the main flow velocity by approximately 20° (Dick and Sleath, 1992; Zala-Flores and Sleath, 1998; Wright, 2002). This means that for low θ_{max}, where ϕ is nearly zero, the erosion depth δ_e lags the near-bed velocity by approximately 20°. It also means that the phase lag between δ_e and the near-bed velocity is as much as 50° for high θ_{max}. These estimates assume that the phase lead between main flow and near-bed flow is the same for low and high

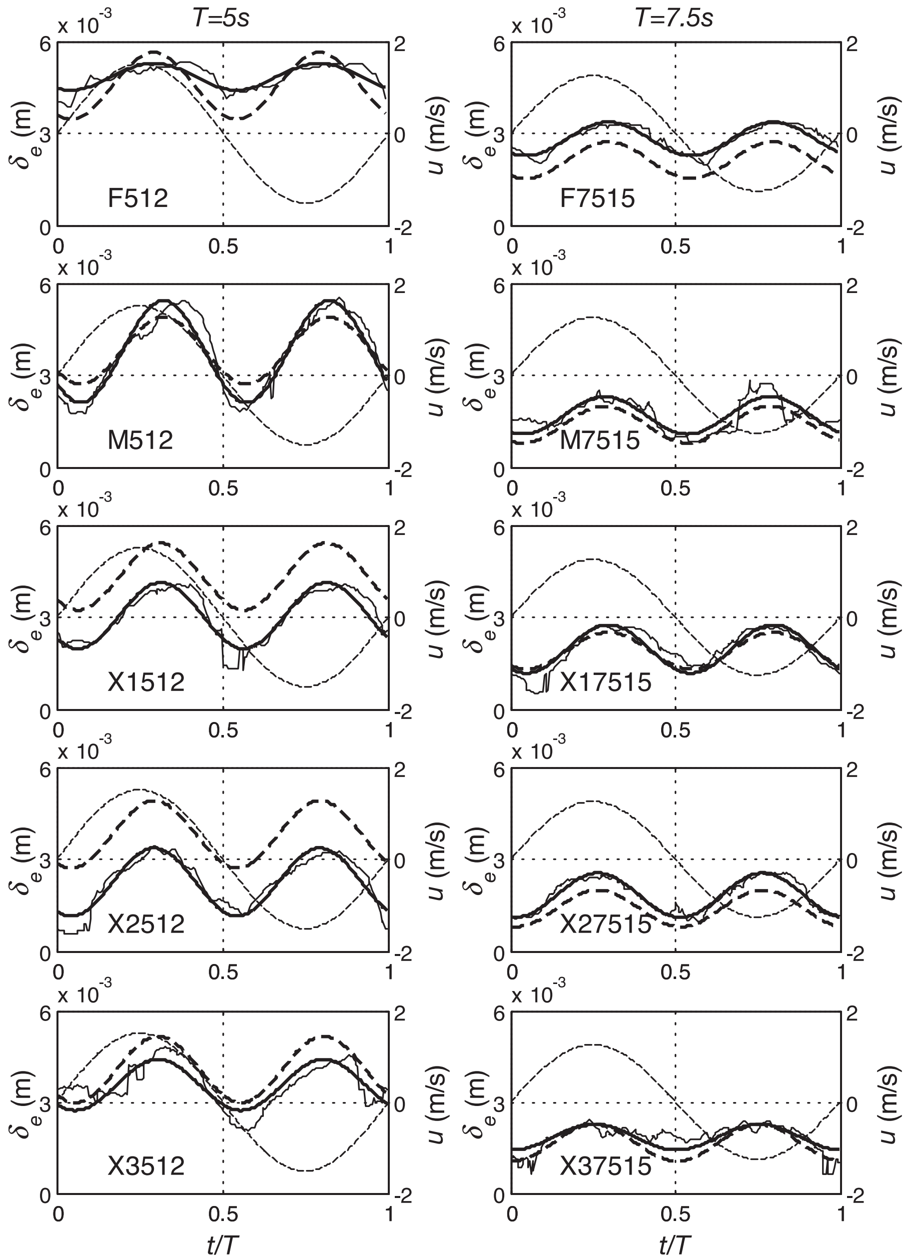

Fig. 6. Time-varying δ_e for sinusoidal flow experiments: — measured δ_e; – – main flow velocity; **—** best fit of Eq. (7); **– –** Eq. (8).

θ_{max}, an assumption that is open to question given the very different sand concentration profiles in the near-bed region. Increasing ϕ for increasing θ_{max} may be due to effects of increased sheet flow layer thickness and concentrations on the near-bed flow. But it may also be due to the much greater erosion depths that occur at higher θ_{max}. For example, results presented later (Eq. (9)) show that maximum erosion depth in the case of $\theta_{max} = 1.5$ is approximately 7 grain diameters while for $\theta_{max} = 6$ maximum erosion depth is approximately 44 grain diameters.

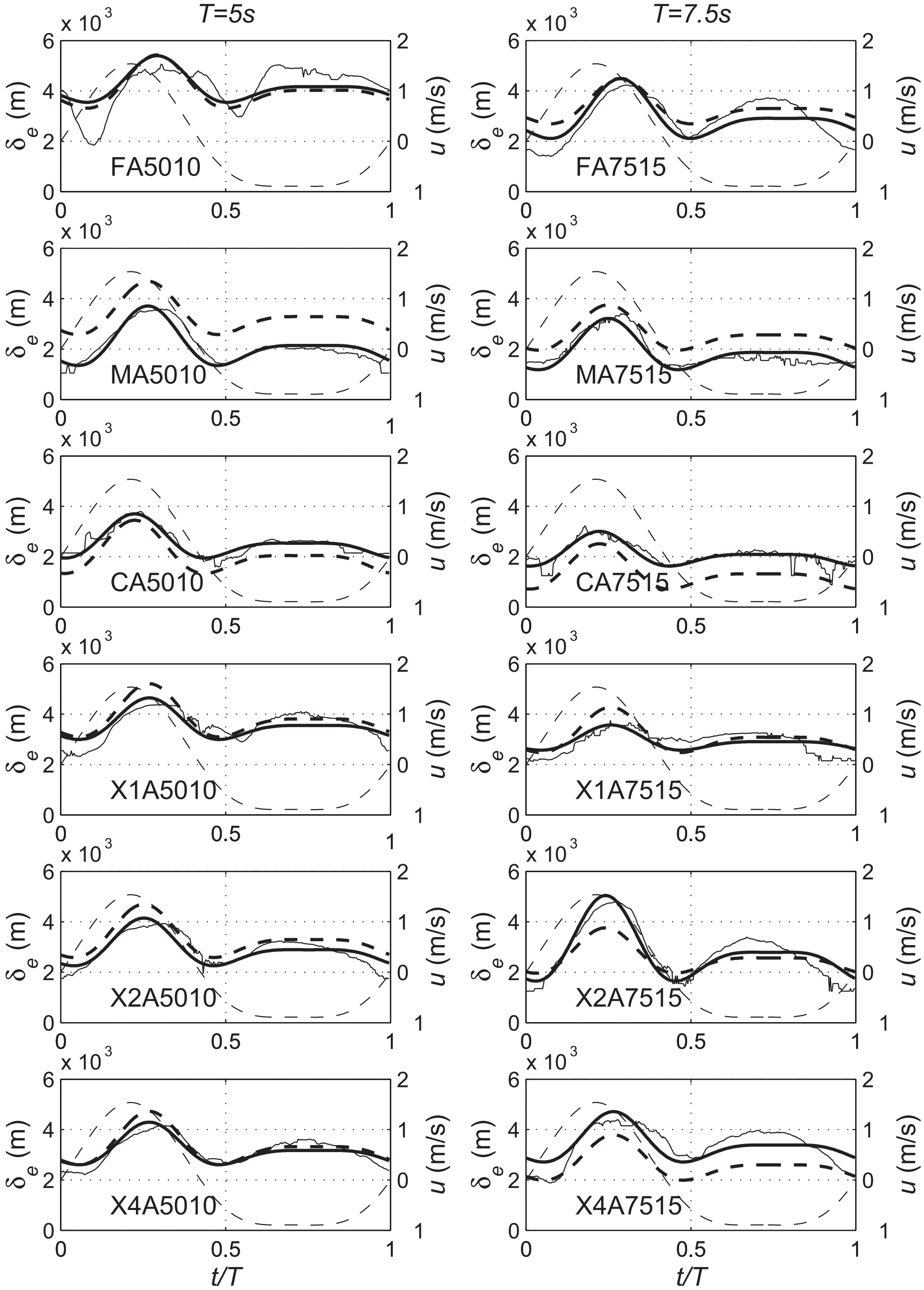

Fig. 7. Time-varying δ_e for asymmetric flow experiments: — measured δ_e; – – main flow velocity; **—** best fit of Eq. (7); **– –** Eq. (8).

A reasonable fit to the results in Fig. 8 is given by

$$\phi = 0.1\theta_{\max} \tag{6}$$

Results which deviate significantly from this fit correspond to cases where the phase lag is difficult to determine accurately because of the "flattened" shape of the δ_e time-series. These results aside, Eq. (6) estimates the phase lag to within ± 0.1 radians.

Previous work has suggested that *maximum* δ_e, normalised by the sediment d_{50}, is proportional to

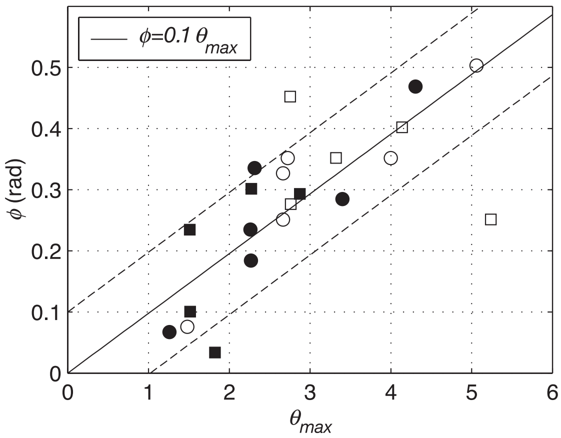

Fig. 8. Erosion depth phase lag, ϕ (○ asymmetric; □ sinusoidal; non-shaded $T=5$ s; shaded $T=7.5$ s).

maximum Shields number for the flow and sediment conditions. The present experiments provide the opportunity to relate time-varying δ_e to time-varying θ. Because θ is in phase with the main flow velocity, u, we relate δ_e to the phase-shifted θ, that is to $\theta\ (\omega t-\phi)$, where $\omega=2\pi/T$ is the flow circular frequency, T being the flow period. Example results are presented in Fig. 9. There are four symbols in each plot of Fig. 9, corresponding to four stages of the asymmetric flow time-history: open circles correspond to the accelerating onshore (positive velocity) part of the flow, closed circles correspond to decelerating onshore flow, open squares correspond to accelerating offshore flow and closed squares correspond to decelerating offshore flow. In the case of the coarse sand, the different symbols cannot be distinguished: in this case δ_e is a simple linear function of θ and we can write

$$\frac{\delta_e(t)}{d_{50}} = C_1\theta(\omega t-\phi)+C_2 \tag{7}$$

where C_1 is the slope of the line through the data and C_2, which measures the erosion depth "offset", is the intercept with the $\delta_e(t)/d_{50}$ axis. In the case of the fine sand, δ_e is not a simple linear function of θ: here we see strong hysteresis with lower δ_e for equivalent θ during positive (onshore) flow acceleration compared with positive flow deceleration. We also see higher δ_e at the on-offshore flow reversal (end of onshore cycle and flow is about to move in offshore direction) compared with the off-onshore flow reversal (when flow is starting to move in the onshore direction). In this case, sand that is suspended by the high velocity onshore flow does not settle back as the onshore velocity decreases to zero and the bed does not recover the level it had at the start of the onshore flow. Strong unsteady effects occur, therefore, in the case of fine sand and Eq. (7) does not properly describe the erosion depth behaviour. Unsteady effects are also evident in the case of the medium sand in Fig. 9 but, as expected, the effects are much weaker than for the fine sand and Eq. (7) gives a reasonably good description of the erosion depth behaviour in this case.

Values of C_1 and C_2 corresponding to the best fit of Eq. (7) to the measured erosion depth time-history for each experiment are listed in Table 3 and the best fits themselves are plotted in Figs. 6 and 7. (Table 3 also includes the values of phase lag, ϕ, obtained from the cross-correlation of $\delta_e(t)$ and $u(t)$ discussed earlier.) It is seen that the fits are generally good but the shortcomings of Eq. (7) in relation to the unsteady effects are seen: a tendency to underestimate erosion depths during decelerating flow and to generally underestimate erosion depths during offshore flow in the case of asymmetric flows. As expected, the shortcomings are

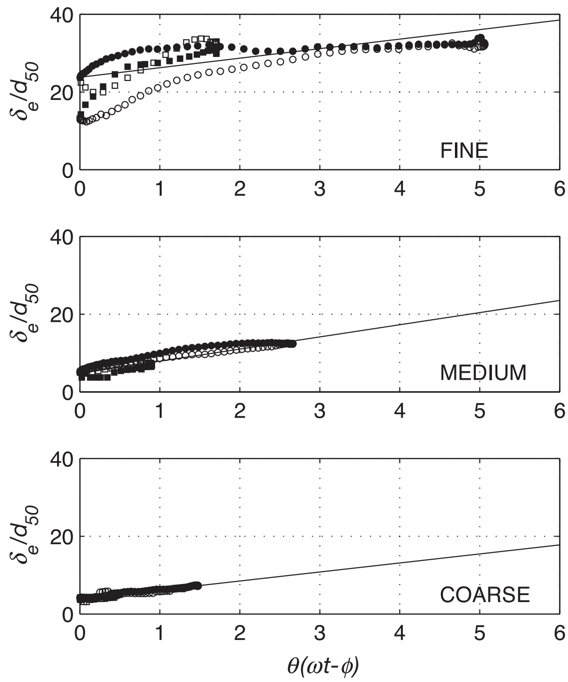

Fig. 9. Instantaneous erosion depth versus instantaneous Shields number for the Fine, Medium and Coarse sands in flow A5010.

Table 3
Empirical coefficients for Eq. (7)

Sinusoidal				Asymmetric			
Exp.	ϕ (rad)	C_1	C_2	Exp.	ϕ (rad)	C_1	C_2
F512	0.25	1.1	29.5	FA5010	0.50	2.4	23.8
F7515	0.39	2.56	15.3	FA7515	0.47	3.7	14.2
M512	0.45	4.3	7.4	MA5010	0.33	3.1	4.8
M7515	0.23	2.9	3.8	MA7515	0.23	3.2	4.2
X1512	0.40	2.9	10.5	CA5010	0.08	2.3	3.8
X17515	0.30	3.7	6.3	CA7515	0.07	2.1	3.2
X2512	0.28	2.8	4.0	X1A5010	0.35	2.2	15.9
X27515	0.10	3.4	3.9	X1A7515	0.28	1.6	13.6
X3512	0.35	2.2	11.6	X2A5010	0.25	2.5	8.0
X37515	0.03	2.0	6.1	X2A7515	0.18	5.3	5.8
				X4A5010	0.35	2.2	9.4
				X4A7515	0.34	3.1	9.8

more pronounced in cases of fine sand and mixed sands containing a significant proportion of fine sand in the mix. In contrast, in the case of the coarse sand, for which unsteady effects will be weakest, the fit of Eq. (7) to the measured $\delta_e(t)$ is excellent.

A comparison of measured $\delta_e(t)$ for the Medium, Mix2 and Mix4 sands shows that the unsteady effects depend on the grading. The sands have the same d_{50} but the grading is very different, with Mix2 and Mix4 containing substantial proportions of fine sand. Fig. 10 shows the comparison for the 5 s asymmetric flow condition. Unsteady effects are seen to be stronger in the mixed sand cases and are strongest in the case of Mix4, which contains the highest proportion of fine sand. A dependence of the erosion depth offset on the grading is also seen with the Mix2 and Mix4 sands having an offset of approximately 2 mm and the Medium sand having an offset of approximately 1 mm.

Eq. (7) can be used as a basis for estimating $\delta_e(t)$ empirically if, like ϕ, C_1 and C_2 can be empirically related to the flow and bed conditions. C_1 and C_2 values are plotted against θ_{max} in Fig. 11. The mean value of C_1 is 2.8 and most points in Fig. 11a are contained in the band $C_1 = 2.8(1 \pm 25\%)$. C_2 increases with increasing θ_{max} in Fig. 11b and the equation $C_2 = 5.5(\theta_{max} - 1)$ estimates C_2 to within $\pm 25\%$ in most cases. (Here, C_2 is zero at $\theta_{max} = 1.0$, recognising that oscillatory sheet flow conditions prevail when $\theta_{max} > \approx 1.0$.) Substitution for C_1 and C_2 in Eq. (7) gives the following empirical equation for time-varying erosion depth:

$$\frac{\delta_e(t)}{d_{50}} = 2.8\theta(\omega t - 0.1\theta_{max}) + 5.5(\theta_{max} - 1) \tag{8}$$

Eq. (8) has been used to calculate $\delta_e(t)$ for the experimental conditions and the results are presented in Figs. 6 and 7. With a few exceptions, Eq. (8) is seen to predict $\delta_e(t)$ very well. The magnitudes and phases of $\delta_e(t)$ are particularly well predicted. Of course the shortcomings of Eq. (7) in relation to unsteady effects are also present in Eq. (8) and so we see the same differences between measured and predicted $\delta_e(t)$ as discussed earlier. In some cases, the most obvious difference between measured and predicted $\delta_e(t)$ is the difference in erosion depth offset, $C_2 d_{50}$. The offset is not likely to be simply a function of θ_{max} as given by Eq. (8); a dependence on flow period, flow shape (sinusoidal or asymmetric) and sand grading might also be expected.

Finally, previous researchers have suggested equations for the maximum erosion depth in oscillatory sheet flow conditions (Asano, 1992; Li and Sawamoto, 1995; Zala-Flores and Sleath, 1998; Dohmen-Janssen, 1999). The equations generally take the form $(\delta_{emax})/(d_{50}) = C\theta_{max}$, where the multiplier C ranges

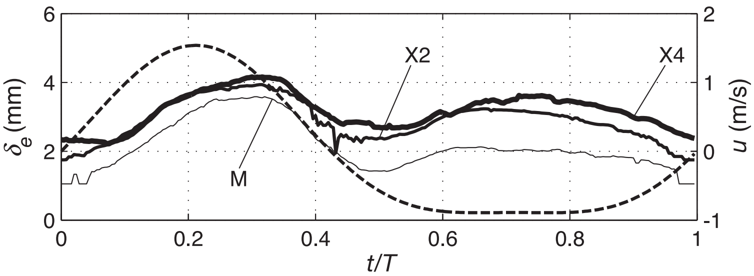

Fig. 10. δ_e for the Medium, Mix2 and Mix4 sands in flow A5010.

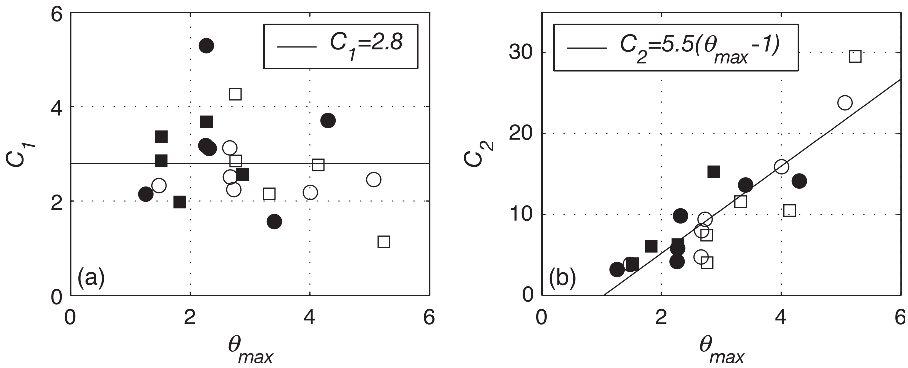

Fig. 11. Empirical coefficients C_1 and C_2 for Eq. (7) (○ asymmetric; □ sinusoidal; non-shaded $T=5$ s; shaded $T=7.5$ s).

from 3 (Zala-Flores and Sleath, 1998 for sand) to 8.5 (Asano, 1992). Fig. 12 presents the measured δ_{emax} from the present study plotted against θ_{max}, along with the δ_{emax} given by Zala-Flores and Sleath (1998), Asano (1992) and the δ_{emax} implied by Eq. (8), i.e.

$$\frac{\delta_{emax}}{d_{50}} = 8.3\theta_{max} - 5.5. \tag{9}$$

The measured θ_{emax} values in Fig. 12 lie between the Zala-Flores and Sleath (1998) and Asano (1992) estimates and are in reasonably good agreement with θ_{emax} given by Eq. (9).

5.1. Reference height and reference concentration

The concentration profile given by Eq. (4) requires the reference concentration, $\bar{c}_a(t)$, at reference height, z_a. Any z where the concentration time-history can be specified is a suitable choice for reference height. Many sediment transport models use reference height $z_a = 2d_{50}$. For this reason, we start the discussion of

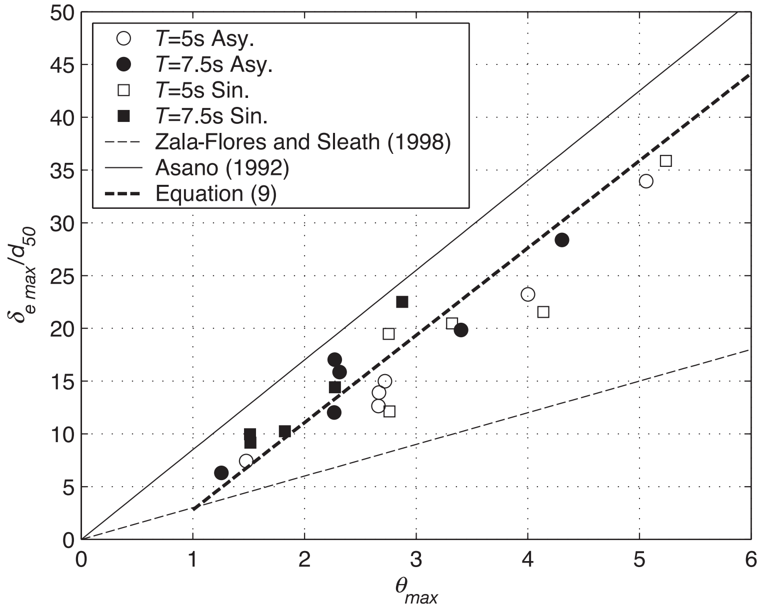

Fig. 12. Maximum erosion depth.

reference height and reference concentration by looking at the concentration time-histories, $\bar{c}\,(t)$, measured at $z = 2d_{50}$. Results for the sinusoidal flow experiments are presented in Fig. 13 and results for the asymmetric flow experiments are presented in Fig. 14.

Consider first the results from the sinusoidal flow experiments (Fig. 13). The measured concentration time-series do not reflect the flow behaviour in that $\bar{c}(t)$ does not exhibit two peaks corresponding to the two peaks in main flow velocity. Indeed, $\bar{c}(t)$ is seen to

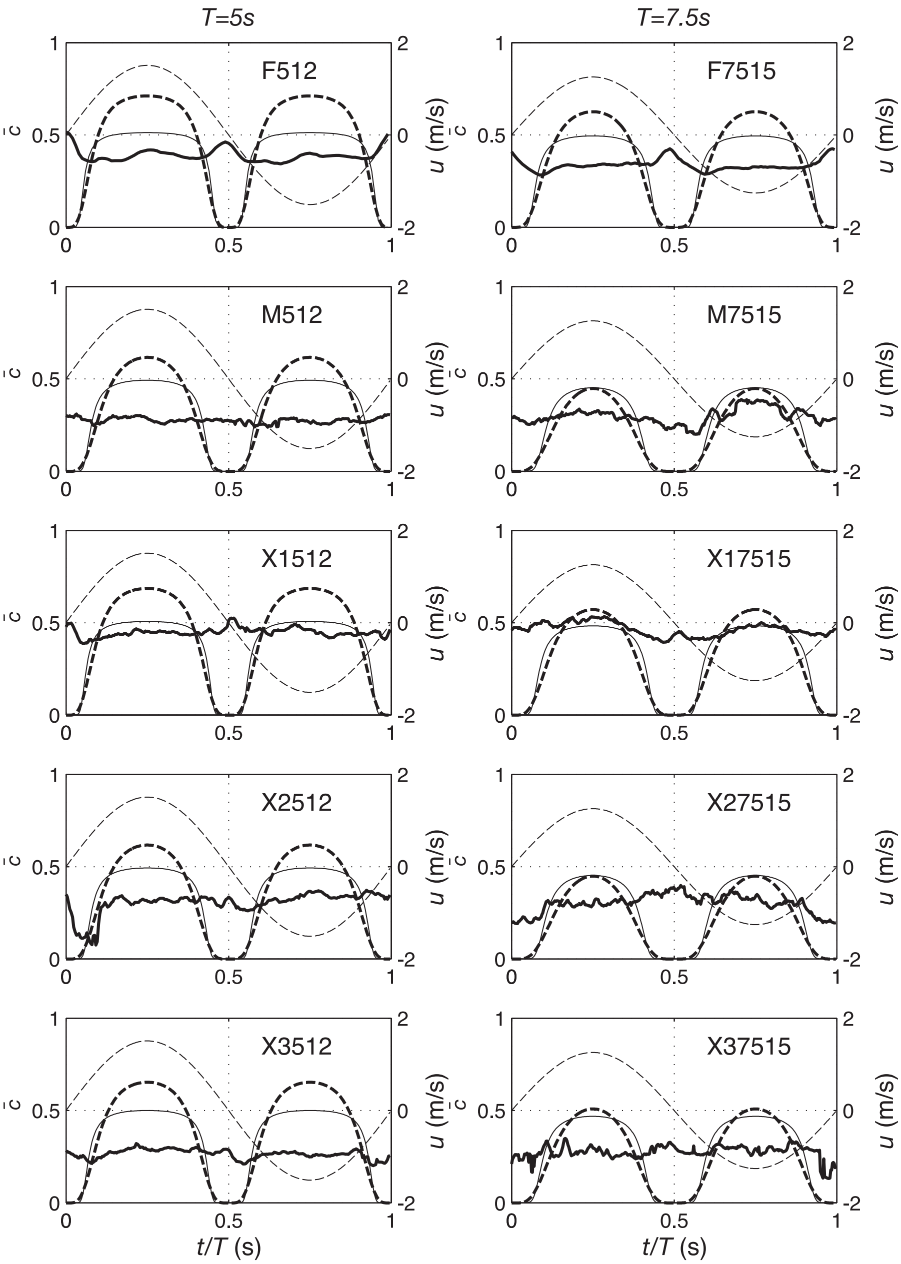

Fig. 13. Concentration at $z = 2d_{50}$ for the sinusoidal flow experiments: – – main flow velocity; — measured $c(t)$ at $z = 2d_{50}$; — Engelund and Fredsøe (1976); – – Zyserman and Fredsøe (1994).

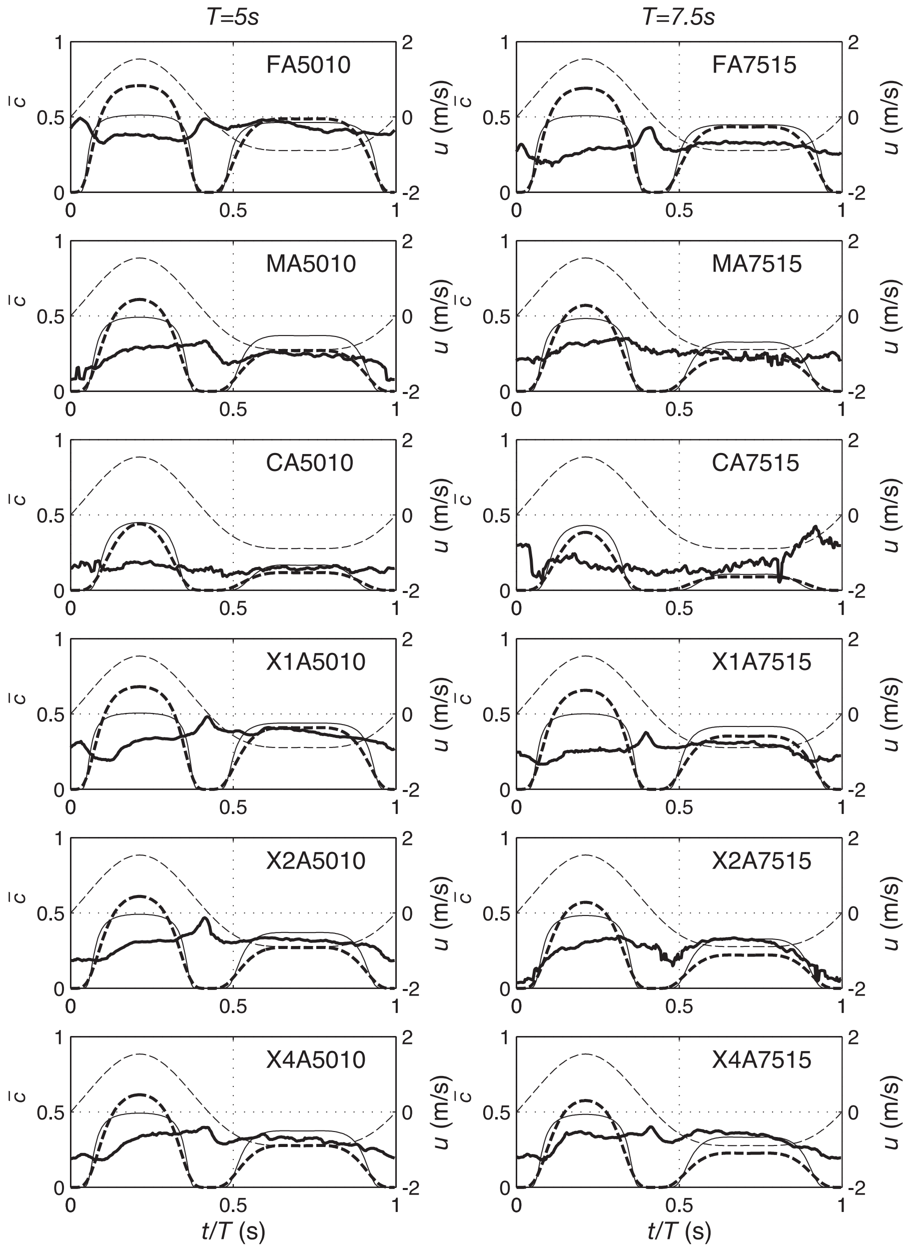

Fig. 14. Concentration at $z=2d_{50}$ for the asymmetric flow experiments: – – main flow velocity; **—** measured *c(t)* at $z=2d_{50}$; — Engelund and Fredsøe (1976); – – Zyserman and Fredsøe (1994).

vary little throughout the flow period and could be considered constant in most cases. Some time-dependence is seen in the fine sand results, which contain a short-duration peak at times of flow reversal, but even here the dynamic range of $\bar{c}(t)$ is low. As described earlier, the top of the pick-up layer corresponds to the boundary between the pick-up layer where the concentration is in anti-phase with the main flow and the upper sheet flow layer where the concentration tends to be in phase with the main flow; concentration at the top of the pick-up layer can, therefore, be expected to be more or less constant. Given that $\bar{c}(t)$ is seen to be reasonably constant in the results presented in Fig. 12, we conclude that, in the case of the sinusoidal flow experiments, the height $z=2d_{50}$ lies *close to* the top of the pick-up layer.

Consider now the results from the asymmetric flow experiments (Fig. 14). In these cases, $\bar{c}(t)$ at $z=2d_{50}$ generally varies during the flow period: concentration increases during the onshore flow, peaks at the offshore flow reversal, decreases rapidly soon after flow reversal before increasing again during the offshore flow. The behaviour indicates that for most of the asymmetric flow experiments, the height $z=2d_{50}$ lies above the pick-up layer.

The location of the top of the pick-up layer for all experiments (sinusoidal and asymmetric) can be found by studying the variation in $\bar{c}_{sd}$ as a function of height z from the bed, where $\bar{c}_{sd}$ is the standard deviation of $\bar{c}(t)$ at z divided by the time-averaged concentration at z. Example results are shown in Fig. 16. $\bar{c}_{sd}$ is zero at maximum erosion depth, it reaches a maximum at about the minimum erosion depth and then decreases to a minimum before increasing again higher in the flow. The point of minimum $\bar{c}_{sd}$ corresponds to the location where the concentration shows the least relative variation during the flow period, i.e. it corresponds to the top of the pick-up layer, denoted z_p. For the examples shown in Fig. 16, we see that $z_p \approx 0$ mm for the sinusoidal flow example while $z_p \approx -1$ mm for the asymmetric flow example. Fig. 17a presents the z_p values obtained in this way for all experiments. The sinusoidal experiments have -0.5 mm $\leq z_p \leq 0.5$ mm, confirming the observation made earlier from Fig. 13 that $z=2d_{50}$ is close to the top of the pick-up layer for the sinusoidal flows. The asymmetric experiments have -1.5 mm $\leq z_p \leq -0.5$ mm, confirming the observation from Fig. 14 that, for the asymmetric flows, $z=2d_{50}$ lies above the top of the pick-up layer.

The fact that the concentration is more or less constant at z_p means that concentration at z_p acts as a fixed point about which the concentration profile pivots during the flow cycle. This is illustrated in Fig. 15. For $z<z_p$, i.e. below the pivot and within the pick-up layer, the concentration decreases as velocity and erosion depth increase; for $z>z_p$, i.e. above the pivot and above the pick-up layer, the concentration increases as velocity and erosion depth increase.

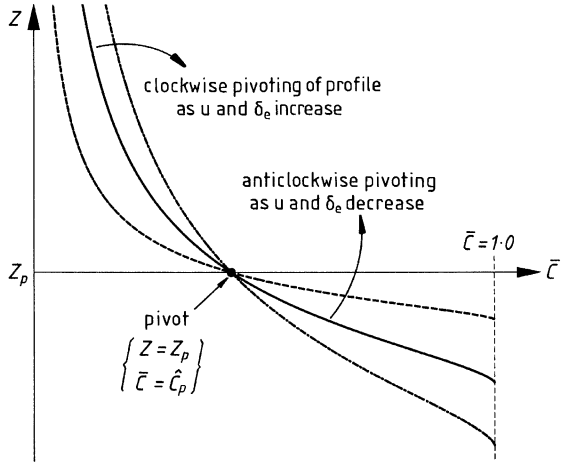

Fig.15. Illustration of concentration profile "pivot".

The near constant concentration at $z=z_p$ makes this height appealing as a choice for the reference height, especially if the value of the constant concentration can be estimated for given flow and bed conditions (Fig. 16). Time-averaged concentrations, $\hat{c}_p$, corresponding to the z_p values in Fig. 17a are presented in Fig. 17b. The results for same sand but different flows show remarkable agreement: $\hat{c}_p$ shows no systematic dependence on flow period, flow magnitude or flow shape. Furthermore, the range of $\hat{c}_p$ is small across the experiments: the average is 0.44 and the standard deviation is 0.08. This analysis suggests that the top of the pick-up layer is a good choice for reference height, i.e. $z_a=z_p$, where z_p lies close to 0 mm for sinusoidal flow and lies close to -1 mm for asymmetric flow; and a reasonable estimate of reference concentration is the time-averaged concentration at z_p, i.e. $\bar{c}_a(t) \approx \hat{c}(z=z_p)=\hat{c}_p \approx 0.44$.

Two of the most commonly used formulae for reference concentration are those of Engelund and Fredsøe (1976) (modified by Fredsøe et al., 1985) and Zyserman and Fredsøe (1994). Both are based on a reference height $z_a=2d_{50}$. The measurements obtained from the present study provide the opportunity to compare reference concentrations predicted by these formulae with measured concentrations. The comparison is presented in Figs. 13 and 14. The formulae are quasi-steady in that $\bar{c}_a(t)$ is always in phase with the main flow velocity. The Engelund and Fredsøe predictions are generally closer to the measurements than

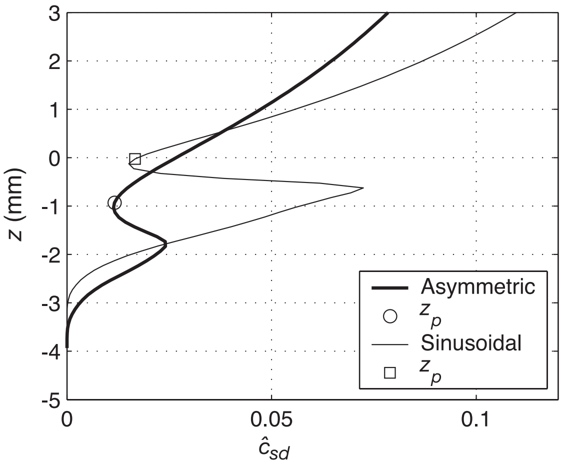

Fig. 16. $\hat{c}_{sd}$ for Mix2 in the $T=5$ s sinusoidal (X2512) and asymmetric flows (X2A512).

the Zyserman and Fredsøe predictions but neither formula is particularly good at predicting the concentration. The most obvious difference between the predicted and measured concentrations is the highly dynamic concentration predicted by the formulae, with $\bar{c}_a=0$ at times of zero velocity, compared with the measured near constant concentration. The amplitude of the predicted dynamic concentration is generally greater than the magnitude of the measured near constant concentration, although agreement is good for the offshore part of the flow cycle in cases of asymmetric flow.

6. Concentration peaks at flow reversal

If $\bar{c}_a$ at reference height z_a is constant with time then according to Eq. (4), the time variation of concentration at all other z is determined by the time variation of the erosion depth, that is by $\delta_e(t)$. (It has already been shown that α in Eq. (4) can be assumed constant with $\alpha = 1.5$.) Within the pick-up layer ($z<z_p$), $\bar{c}(t)$ will be in anti-phase with $\delta_e(t)$ while above the pick-up layer, $\bar{c}(t)$ will be in phase with $\delta_e(t)$. This has already been seen in Fig. 3 and is shown more clearly in Fig. 18. For experiments FA7515 and X4A5010, Fig. 18 presents the measured $\bar{c}(t)$ for five elevations (indicated by the z-value in each graph) where the time-averaged normalised concentrations are $\hat{c}=0.75$, 0.6, 0.44, 0.25 and 0.125. Also shown are the corres-ponding $\bar{c}(t)$ calculated using Eq. (4) with the follo-wing input: the measured $\delta_e(t)$; the measured z_p (-0.4 and -1.4 mm for the FA7515 and X4A5010 experiments, respectively) for the reference height z_a; and the measured $\hat{c}_p$ (0.39 and 0.57 for the FA7515 and X4A5010 experiments, respectively) for the reference concentra-

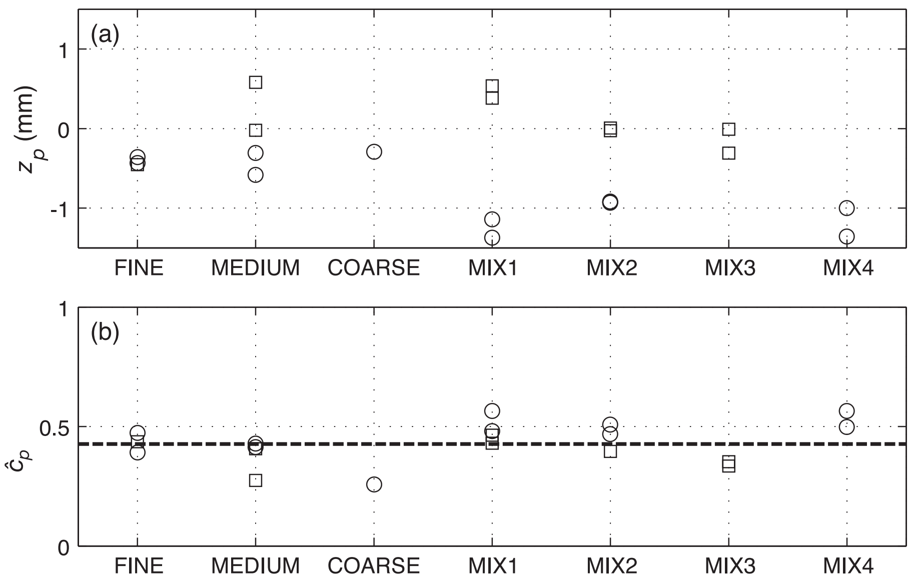

Fig. 17. Measured values of z_p and $\hat{c}_p$ (○ asymmetric flows; □ sinusoidal flows).

tion $\bar{c}_a(t)$. Agreement between the measured and calculated $\bar{c}(t)$ is very good and the time-series show the expected behaviour, i.e. $\bar{c}(t)$ in anti-phase with $\delta_e(t)$ for $z<z_p$ and $\bar{c}(t)$ in phase with $\delta_e(t)$ for $z>z_p$.

There are, however, some differences between the measured and calculated $\bar{c}(t)$ in Fig. 18. In particular, the measured $\bar{c}(t)$ show a peak in concentration close to flow reversal, which is absent from the calculated $\bar{c}(t)$. The peak is very obvious above the pick-up layer and is smaller but still noticeable within the pick-up layer. The flow reversal peaks within and above the pick-up layer are in phase, unlike peaks at other times in the flow cycle, and there is no noticeable peak in erosion depth to match the flow reversal peak. The flow reversal peak is, therefore, associated with a short-duration clockwise pivoting of the concentration profile about the erosion depth level, producing a short-duration increase in concentration over the whole sheet flow layer before falling back again to continue its normal pivoting about the z_p level. The calculated concentration time-series in Fig. 18 does not show the flow reversal peaks because reference concentration is constant with time in the calculations ($\bar{c}_a(t)=\hat{c}_p$).

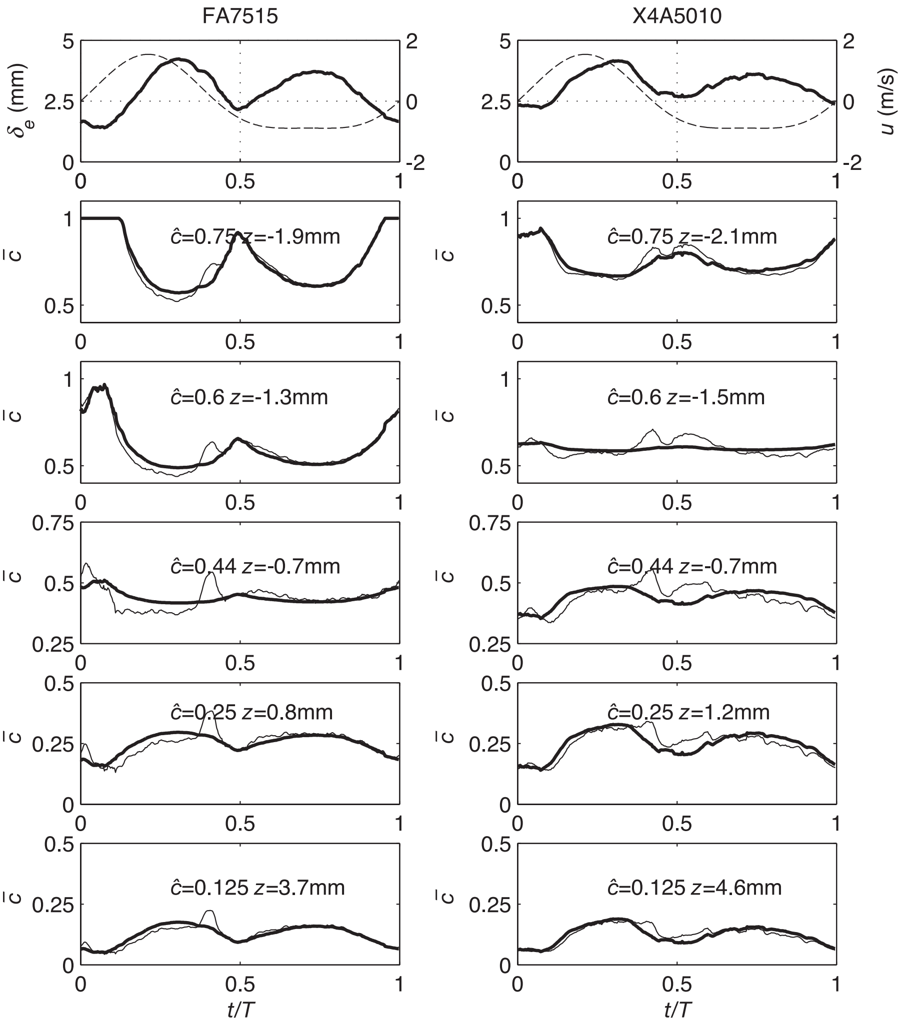

Fig. 18. Top panels: measured $\delta_e(t)$ and main flow velocity for experiments FA7515 and X4A5010; other panels: corresponding $\bar{c}(t)$ measured (–) and calculated (—) using Eq. (4).

Flow reversal peaks near the top of the sheet flow layer have been observed in other flow tunnel experiments (e.g. Murray et al., 1991; Ribberink and Al-Salem, 1992; Ribberink and Chen, 1993; Katopodi et al., 1994; Janssen and Ribberink, 1996; Nihei et al., 1999; Rose et al., 1999; McLean et al., 2001; Doh-

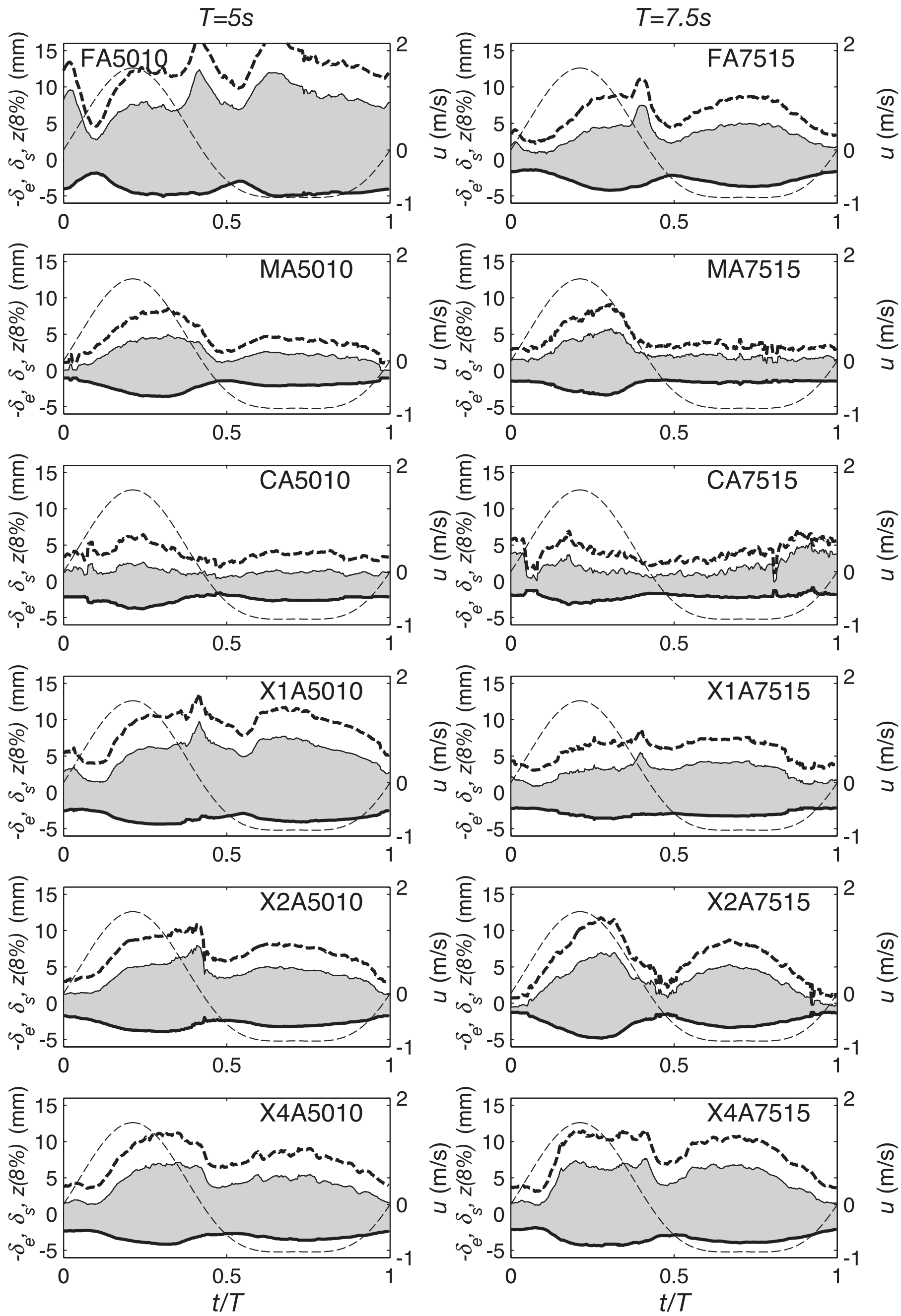

Fig. 19. Main flow velocity (– –), sheet flow layer thickness $\delta_s(t)$ (— —), z corresponding to 8% concentration (–) and $-\delta_e(t)$ (—) for the asymmetric flow experiments.

men-Janssen et al., 2002) and the physical mechanisms causing the peaks have been the subject of much speculation. The present experiments show that the concentration peak at flow reversal, while most obvious at the top of the sheet flow layer, persists down into the sheet flow layer and is not matched by a corresponding peak in erosion depth. It seems possible therefore that the concentration peak is caused by settling of sediment from elevations higher in the flow. The fact that the peaks are strongest in cases of fine sand and at times of on-offshore flow reversal of asymmetric flows supports this hypothesis: under such conditions, significant volumes of sand are present in the flow above the sheet flow layer, having been suspended to high levels by the preceding high-velocity onshore flow. Although the peaks are interesting, they have little impact on net sediment transport within the sheet flow layer because of their short duration and because flow velocities are low at the time of their occurrence.

7. Sheet flow layer thickness

While the erosion depth obviously defines the bottom of the sheet flow layer, there is no generally accepted definition for the top of the sheet flow layer. Dohmen-Janssen (1999) suggests that the upper sheet flow boundary could be defined as the level in the flow where the volumetric concentration is 8% (i.e. $\bar{c}=0.13$) because average grain spacing is approximately one grain diameter at this concentration and, therefore, grain-to-grain interactions are negligible. Fig. 19 presents the measured time-dependent sheet flow layer thickness, $\delta_s(t)$, based on the 8% definition, for the asymmetric flow experiments. The shaded area in each graph of Fig. 19 is the sheet flow layer, the thick-lined bottom boundary is the erosion depth and the thin-lined top boundary is the height of the 8% concentration; the thick broken line in each graph is the sheet flow layer thickness, $\delta_s(t)$, and the thin dashed line is the main flow velocity.

Fig. 19 does not provide any additional concentration results to what has already been presented; it simply provides a nice illustration of the sheet flow layer through the flow cycle. The sheet flow layer plots in Fig. 19 reflect the concentration results already presented. We see that the thickness of the sheet flow layer is greatest for the fine sand and smallest for the coarse sand. For example, in flow A5010, the maximum layer thickness in the case of fine sand is 17 mm, in the case of the medium sand, it is 8 mm and in the case of the coarse sand, it is 5 mm. Grading plays a substantial role in sheet flow layer thickness: the medium, Mix2 and Mix4 sands have the same d_{50} but sheet flow layer thickness is much greater in the Mix2 and Mix4 cases because of the presence of fine sand in the mixes. Finally, short-duration peaks in sheet flow layer thickness are observed at the on-offshore flow reversal and, as discussed earlier, are most obvious in cases of fine sand and mixes containing a large percentage of fine sand.

8. Conclusions

To date, the description of time-dependent concentrations in oscillatory sheet flow based on experimental data has been largely qualitative. The range and level of detail in concentration measurements from the present study make it possible to study the concentrations more rigorously and to do so in a quantitative manner. Analysis of the data has led to the following main conclusions:

(1) The time-varying concentration profile in the sheet flow layer is well characterised by a new equation (Eq. (4)) involving two variables: the erosion depth and the reference concentration.
(2) Erosion depth lags the main flow and is never zero during the flow cycle. To a first approximation, time-varying erosion depth can be directly related to time-varying Shields number (Eq. (8)). However, grading effects play a part in determining erosion depth. Unsteady effects become increasingly important as the percentage of fine sand in the bed increases and the proposed empirical equation then constitutes a less accurate description of the time-varying erosion depth.
(3) Reference height for reference concentration is best taken at the top of the pick-up layer, where concentration is reasonably constant throughout the flow cycle. The top of the pick-up layer lies close to $z \approx 0$ mm for sinusoidal flow and close to $z \approx -1$ mm for asymmetric flow. To a first approximation, reference normalised concentra-

tion at the top of the pick-up layer can be taken as constant with $\bar{c} = 0.44$.

(4) Well-known quasi-steady reference concentration formulae predict very dynamic concentration at $z = 2d_{50}$. In contrast, the measurements show that $z = 2d_{50}$ is not far from the top of the pick-up layer where concentration is nearly constant throughout the flow cycle.

(5) As observed by others, a short-duration peak in concentration occurs at flow reversal. The peak is strongest in cases of fine sand and at the on-offshore flow reversal of asymmetric flows. It occurs throughout the sheet flow layer and is most obvious at the top of the sheet flow layer.

The research has produced a large dataset containing measurements of transport processes in full-scale sinusoidal and asymmetric oscillatory sheet flow conditions. The present paper has focussed on the sheet flow concentrations; later papers will focus on sand fluxes and sand transport. The overall objective of the research has been to obtain good measures of sheet flow sand transport processes at large-scale and to use the data to (i) establish empirical descriptions of the underlying processes and (ii) develop and test process-based numerical models. To facilitate the latter, a database of the experimental data has been produced and is available on request to the corresponding author.

Acknowledgements

The research was carried out with funding from the UK Engineering and Physical Sciences Research Council (EPSRC Grants GR/M75563, GR/R23572). The Malvern particle size analyser was borrowed from the EPSRC's equipment loan pool. As always, thanks go to the Fluids Laboratory technician Rab Fraser and the other technical staff at Aberdeen University.

Appendix A. Notation

A	amplitude of main flow horizontal excursion
a	asymmetry in main flow horizontal velocity
C, C_1, C_2	empirical constants
c	sediment concentration
c_a	reference concentration at reference height z_a
c_o	sediment concentration in undisturbed bed (1600 g/l)
$\bar{c}$	normalised concentration, c/c_o
$\bar{c}_{sd}$	standard deviation of $\bar{c}$, divided by $\hat{c}$
$\hat{c}$	time-averaged, normalised concentration
$\hat{c}_p$	time-averaged, normalised concentration at top of pick-up layer z_p
d_{10}, d_{50}, d_{90}	size for which 10%, 50%, 90% of the sediment sample is finer
f_w	friction factor
g	acceleration due to gravity
s	sediment specific gravity
t	time
T	flow period
u	main flow horizontal velocity
u_{max}, u_{min}	maximum, minimum main flow horizontal velocity
u_{rms}	root mean square main flow horizontal velocity
z	vertical coordinate relative to undisturbed bed level
z_a	reference height for reference concentration
z_p	vertical location of top of pick-up layer
α, β	parameters for concentration profile equation
δ_e	erosion depth
δ_s	sheet flow layer thickness
ϕ	phase difference between main flow and erosion depth
θ	shields number
ω	flow angular frequency ($= 2\pi/T$)

References

Asano, T., 1992. Observations of granular-fluid mixture under an oscillatory sheet flow. ASCE, Proceedings 23rd International Conference on Coastal Engineering, 1896–1909.

Chatelus, Y., Katopodi, I., Dohmen-Janssen, M., Ribberink, J.S., Samothrakis, P., Cloin, B., Savioli, J.C., Bosboom, J., O'Connor, B.A., Hein, R., Hamm, L., 1998. Size gradation in sediment transport. ASCE, Proceedings 26th International Conference on Coastal Engineering, 2435–2448.

Clubb, G.S., 2001. Experimental study of vortex ripples in full scale sinusoidal and asymmetric flows. PhD Thesis. University of Aberdeen.

Davies, A.G., van Rijn, L.C., Damgaard, J.S., van de Graaff, J., Ribberink, J.S., 2002. Intercomparison of research and practical sand transport models. Coastal Engineering 46, 1–23.

Dick, J.E., Sleath, J.F.A., 1992. Sediment transport in oscillatory sheet flow. Journal of Geophysical Research 97, 5745–5758.

Dohmen-Janssen, C.M., 1999. Grain size influence on sediment transport in oscillatory sheet flow: phase lags and mobile bed effects. PhD Thesis. Delft University of Technology.

Dohmen-Janssen, C.M., Kroekenstoel, D.F., Hassan, W.N., Ribberink, J.S., 2002. Phase lags in oscillatory sheet flow: experiments and bed load modelling. Coastal Engineering 46, 61–87.

Engelund, F., Fredsøe, J., 1976. A sediment transport model for straight alluvial channels. Nordic Hydrology 7, 295–324.

Fredsøe, J., Andersen, O.H., Silberg, S., 1985. Distribution of suspended sediment in large waves. ASCE, Journal of Waterway, Port, Coastal and Ocean Engineering 111 (6), 1041–1059.

Horikawa, K., Watanabe, A., Katori, S., 1982. Sediment transport under sheet flow condition. ASCE, Proceedings 19th International Conference on Coastal Engineering, 1335–1352.

Janssen, C.M., Ribberink, J.S., 1996. Grain size influence on sand transport in oscillatory sheet flow. ASCE, Proceedings 26th International Conference on Coastal Engineering, 4779–4792.

Katopodi, I., Ribberink, J.S., Ruol, P., Lodahl, C., 1994. Sediment transport measurements in combined wave-current flows. ASCE, Proceedings 1st International Conference on Coastal Dynamics, 837–851.

Li, L., Sawamoto, M., 1995. Experiments on sediment transport in sheet-flow regime under oscillatory flow. Coastal Engineering in Japan 38 (2), 143–156.

McLean, S.R., Ribberink, J.S., Dohmen-Janssen, C.M., Hassan, W.N., 2001. Sand transport in oscillatory sheet flow with mean current. ASCE, Journal of Waterway, Port, Coastal and Ocean Engineering 127 (3), 141–151.

Murray, P.B., Davies, A.G., Soulsby, R.L., 1991. Sediment pick-up in wave and current flows. In: Soulsby, R., Bettess, R. (Eds.), Sand Transport in Rivers, Estuaries and the Sea. Euromech, vol. 262. A.A Balkema, Rotterdam, The Netherlands, 37–43.

Nihei, Y., Nadaoka, K., Nakamura, N., 1999. Laboratory experiments and LES computation of sheet-flow turbulence under oscillatory flows. ASCE, Proceedings of the 4th International Conference on Coastal Sediments, 108–118.

Ribberink, J.S., Al-Salem, A.A., 1992. Time-dependent sediment transport phenomena in oscillatory boundary layers under sheet flow conditions. Delft Hydraulics Report H840.20, part VI.

Ribberink, J.S., Al-Salem, A.A., 1995. Sheet flow and suspension of sand in oscillatory boundary layers. Coastal Engineering 25, 205–225.

Ribberink, J.S., Chen, Z., 1993. Sediment transport of fine sand under asymmetric oscillatory flow. Delft Hydraulics Report H840, part VII.

Rose, C.P., Trouw, K., Cloin, B., Arnott, A.D., Sistermans, P.G.J, van de Graaff, J., Dong, P., Ribberink, J.S., O'Connor, B.A., 1999. Vertical sediment entrainment characteristics in oscillatory sheet flow conditions. ASCE, Proceedings of the 4th International Conference on Coastal Sediments, 135–147.

Sleath, J.F.A., 1999. Conditions for plug formation in oscillatory flow. Continental Shelf Research 19, 1643–1664.

Wilson, K.C., Andersen, J.S., Shaw, J.K., 1995. Effects of wave asymmetry on sheet flow. Coastal Engineering 25, 191–204.

Wright, S., 2002. Well-sorted and graded sands in oscillatory sheet-flow. PhD Thesis. University of Aberdeen.

Wright, S., O'Donoghue, T., 2002. Graded sediments in oscillatory sheet-flow. ASCE, Proceedings 28th International Coastal Engineering Conference, 2638–2650.

Zala-Flores, N., Sleath, J.F.A., 1998. Mobile layer in oscillatory sheet flow. Journal of Geophysical Research 103 (C6), 12783–12793.

Zyserman, J.A., Fredsøe, J., 1994. Data analysis of bed concentration of suspended sediment. ASCE, Journal of Hydraulic Engineering 120 (9), 1021–1042.